A peptide fragment of azurin induces a p53-mediated cell cycle arrest in human breast cancer cells

Tohru Yamada,[1] Rajeshwari R. Mehta,[1] Fatima Lekmine,[1] Konstantin Christov,[1] Marissa L. King,[2] Dibyen Majumdar,[2] Anne Shilkaitis,[1] Albert Green,[1] Laura Bratescu,[1] Craig W. Beattie,[1] and Tapas K. Das Gupta[1]

Departments of [1]Surgical Oncology and [2]Mathematics, Statistics, and Computer Sciences, University of Illinois College of Medicine, Chicago, Illinois

Abstract

We report that amino acids 50 to 77 of azurin (p28) preferentially enter the human breast cancer cell lines MCF-7, ZR-75-1, and T47D through a caveolin-mediated pathway. Although p28 enters p53 wild-type MCF-7 and the isogenic p53 dominant-negative MDD2 breast cancer cell lines, p28 only induces a G_2-M-phase cell cycle arrest and apoptosis in MCF-7 cells. p28 exerts its antiproliferative activity by reducing proteasomal degradation of p53 through formation of a p28:p53 complex within a hydrophobic DNA-binding domain (amino acids 80-276), increasing p53 levels and DNA-binding activity. Subsequent elevation of the cyclin-dependent kinase inhibitors p21 and p27 reduces cyclin-dependent kinase 2 and cyclin A levels in a time-dependent manner in MCF-7 cells but not in MDD2 cells. These results suggest that p28 and similar peptides that significantly reduce proteasomal degradation of p53 by a MDM2-independent pathway(s) may provide a unique series of cytostatic and cytotoxic (apoptotic) chemotherapeutic agents. [Mol Cancer Ther 2009;8(10):2947–58]

Introduction

Azurin, a member of the cupredoxin family of redox proteins present in bacteria and green plants, is a type I copper-containing soluble protein (10-14 kDa) that transports electrons during denitrification and photosynthesis (1). We and others have shown that azurin preferentially enters cancer cells (2–5) and induces a p53-mediated apoptosis in murine J774, human breast cancer, melanoma (2, 3, 5), and osteosarcoma cells but not in p53-negative osteosarcoma and normal liver cells (p53 wild-type; ref. 6). Azurin also inhibits the proliferation of p53 wild-type breast and melanoma xenografts in athymic mice (3, 5) possibly by stabilizing intracellular levels of p53 (3, 5). Microcalorimetry studies suggest that azurin binds to the NH_2-terminal domain of p53 with nanomolar affinity in a 4:1 stoichiometry (7). Additional observations also suggest that azurin binds to the NH_2-terminal domain and DNA-binding domain (DBD), which include amino acids 1 to 292, but not the COOH-terminal region of p53 (5, 7), and that the azurin:p53 complex is stable (8). Docking and free energy studies show azurin binding to the flexible L_1 and s_7–s_8 loops of the p53 DBD and stabilizing them through tight protein-protein packing interactions (9). Site-directed mutagenesis of azurin also indicates that the region interacting with p53 contains amino acids Met^{44} and Met^{64}, located in a hydrophobic patch of the protein. This region appears critical for formation of a p53 complex (3) and may be key to stabilizing the flexible L_1 and s_7-s_8 motifs of p53 (9). It may also be critical to understanding the mechanism underlying the antiproliferative activity of azurin (3, 5).

Amino acids 50 to 77 of azurin (p28), which encompass Met^{64}, essentially act as a protein transport domain for azurin (10). We refined the protein transport domain to amino acids 50 to 67 of azurin (p18) and suggested that the COOH-terminal 10 to 12 amino acids of p28 were responsible for its antiproliferative activity (11). Here, we show how p28 accounts for a significant amount of the overall tumoricidal activity of azurin *in vitro* and *in vivo* by binding to and increasing intracellular levels of p53, elevating the cyclin-dependent kinase (CDK) inhibitors p21 and p27, and inhibiting cell cycle at G_2-M in a time-dependent manner.

Materials and Methods

Cell Culture

The human breast cancer cell lines used were MCF-7 (p53 wild-type), MCF-10A (p53 wild-type), ZR-75-1 (p53 wild-type), T47D (p53 mutant; American Type Culture Collection), and MDD2 (p53 dominant-negative; courtesy of Dr. Andrei V. Gudkov, Roswell Park Cancer Institute); cells were cultured in MEM-E (Invitrogen) containing 2 mmol/L L-glutamine and 0.1 mmol/L essential amino acids supplemented with 10% heat-inactivated fetal bovine serum (3, 5, 11).

Bacterial Culture and Isolation of Azurin

Escherichia coli JM109 culture and wild-type azurin purification steps were as described (2).

Received 5/19/09; revised 8/25/09; accepted 8/26/09; published OnlineFirst 10/6/09.

Grant support: Sponsored research agreement between CDG Therapeutics and the University of Illinois at Chicago.

The costs of publication of this article were defrayed in part by the payment of page charges. This article must therefore be hereby marked *advertisement* in accordance with 18 U.S.C. Section 1734 solely to indicate this fact.

Requests for reprints: Tapas K. Das Gupta, 840 South Wood Street, Chicago, IL 60612. Phone: 312-996-6134; Fax: 312-996-9365. E-mail: TKDG@uic.edu

doi:10.1158/1535-7163.MCT-09-0444

Peptide Synthesis

All azurin-derived peptides including p18 (Leu^{50}-Gly^{67} LSTAADMQGVVTDGMASG), p28 (Leu^{50}-Asp^{77} LSTAADMQGVVTDGMASGLDKDYLKPDD), p18b (Val^{60}-Asp^{77} VTDGMASGLDKDYLKPDD), p12 (Gly^{66}-Asp^{77} SGLDKDYLKPDD), and poly-arginine (Arg_8) were synthesized by CS Bio at >95% purity and mass balance.

Cell Proliferation Assays

The effect of p28 on cell proliferation was determined as described (11). Briefly, cells were seeded into 24-well plates (Becton Dickinson) and incubated overnight at 37°C. Culture medium containing p28 at 5 to 200 μmol/L was changed daily. After p28 treatment, trypsinized cells were counted using a Beckman Coulter (Z1 coulter particle counter). The cells without p28 added in the wells were used as control (100%). Estradiol-pretreated (0.72 mg/pellet, 60-day release; Innovative Research) female athymic mice (Harlan; 4-5 weeks old) received 3×10^6 MCF-7 cells s.c. on the right flank. Mice were randomized into control and experimental groups when xenograft tumors reached 1 to 2 mm in diameter (5). Control animals received either PBS/castor oil i.p.; 12.8 mg/kg (15 μmol/kg) paclitaxel in PBS/castor oil i.p. on days 10, 14, 21, and 25 post-tumor development (12); or 5 mg/kg (1.7 μmol/kg) or 10 mg/kg (3.4 μmol/kg) p28 in sterile PBS i.p. daily for 30 days. Tumor volume was determined three times a week (3, 5). Body weights were measured twice weekly. Mice were necropsied on day 31 and all tumors were excised and processed for histopathology and immunocytochemistry. Significance ($P < 0.05$) between control and treated groups was determined using a series of mixed-model analyses as described previously (5). A log-quadratic mixed-model fit the data and identified 10 mg/kg p28 as significantly different than control.

Immunocytochemistry

Bromodeoxyuridine (BrdUrd; 50 mg/kg body weight) was injected i.p. 2 h before necropsy to identify dividing cells. Tumor cell nuclei labeled with BrdUrd were identified with an anti-BrdUrd monoclonal antibody (Becton Dickinson). p53 expression was assessed in formalin-fixed, 5 μm paraffin sections with p53 antibody (DO-1; Santa Cruz Biotechnology) and rat anti-mouse IgG2a as the second antibody. Cells expressing p53 were identified with Vectastain Elite ABC kit (Vector Laboratories) and 3,3′-diaminobenzidine tetrahydrochloride (Sigma-Aldrich). Slides were counterstained with hematoxylin. Ten nonoverlapping fields (250 cells per field) from each tumor periphery were counted (40×) for p53-labeled cells (13).

Cell Penetration Studies by Confocal Microscopy and Fluorescence-Activated Cell Sorting

Cell penetration studies and inhibitor conditions were as described (11). At least 10,000 cells were analyzed by fluorescence-activated cell sorting (FACS; red fluorescence; FL-8 filter) and mean fluorescence intensity (MFI) was calculated. Data are presented as mean ± SE of three independent observations. Cyclin B1 and p21 staining were done on fixed cells, permeabilized with methanol and acetone, washed with PBS, and incubated with anti-p21 or anti-cyclin B1 at 1:200 dilution. Secondary antibody conjugated to Alexa Fluor 568 was used at 1:100 dilution (11). Images were taken using an inverted confocal laser scanning microscope (model LC510; Carl Zeiss).

Kinetics of p28 Entry

MCF-7, MCF-10A, and MDD2 cells (3×10^5) were suspended in MEM-E without phenol red. Reactions were started by adding Alexa Fluor 568–conjugated p28 at 10 to 300 μmol/L for 30, 60, 90, and 120 s on ice. After incubation, 1 mL cold PBS was added to each reaction tube and cells were centrifuged twice at $600 \times g$ at 4°C for 2 min. Fixed cells were analyzed for each time point and concentration by FACS and background and relative fluorescence were calculated (11).

Cell Cycle Analysis

MCF-7 and MDD2 cells were incubated with 50 μmol/L of p28 for 48 and 72 h at 37°C, washed with PBS, and fixed in 70% ethanol at −20°C. Fixed cells were washed with PBS and stained by 50 μg/mL propidium iodide in PBS containing 20 μg/mL RNase A (4). Flow cytometry (EPICS Elite ESP; Beckman Coulter) was used to determine DNA content. A minimum of 10,000 cells were collected in each experiment.

Immunoblotting and Immunoprecipitation Analyses

MCF-7 and MDD2 cells were cultured with 50 μmol/L p28 for 24, 48, and 72 h and whole-cell lysates were prepared as described earlier (2). Phosphorylated cdc2 was analyzed in cell lysates prepared in 10 mmol/L NaF, 137 mmol/L NaCl, 1 mmol/L $NaVO_4$, 10 mmol/L EDTA, 1% NP-40, 1 mmol/L DTT, and proteinase inhibitors (Sigma-Aldrich). Caveolin-enriched fractions were prepared as described (14, 15). Briefly, MCF-7 cells were incubated in the presence or absence of 50 μmol/L p28 for 0 (control), 5, 30, and 60 min at 37°C. Washed cells (PBS) were homogenized, samples adjusted to 45% sucrose, and placed at the bottom of the ultracentrifuge tubes. A 5% to 35% discontinuous sucrose gradient was formed above and centrifuged at $200{,}000 \times g$ for 20 h at 4°C. Each fraction was collected and used for immunoblotting. Ubiquitinated p53 was detected as described (16, 17). MCF-7 cells were cultured with p28 at 50 μmol/L for 24, 48, and 72 h in the absence or presence of the proteasome inhibitor MG132 (Sigma-Aldrich) for 7 h before harvesting (18). Equal amounts of protein were immunoprecipitated from whole-cell lysates for Western analysis with anti-p53 antibody. Whole-cell lysates were also subjected to Western analysis with anti-actin antibody as a loading control. Immunocomplexes were washed twice, separated on a 4% to 12% gel, and transferred to a polyvinylidene difluoride membrane. Antibodies against p53 (DO-1 and FL393), p27, CDKs, cyclins (Santa Cruz Biotechnology), and p21 (Invitrogen) were used according to the suppliers' instructions. Actin expression was determined with a monoclonal actin antibody (Santa Cruz Biotechnology), and protein bands were visualized using ECL reagent (Santa Cruz Biotechnology).

Anti-p28 Antibody

We introduced a cysteine at the NH_2 terminus of p28 (CS Bio), conjugated the peptide with keyhole limpet

hemocyanin through the thiol groups of the cysteine residue, and generated a polyclonal antibody in rabbits (New Zealand White). Antibody titer was determined by direct ELISA using p28 (0-3 μg/well). An antibody dilution of 1:140,000 was sufficient to give a reproducible change in absorbance of 0.5 at 450 nm after 15 min incubation with substrate (1-Step PNPP; Pierce) at 25°C when 96-well plates (Nunc) were coated with 1 μg/well p28.

GST Pull-down and Competition Assays

p28 binding to p53 was analyzed using a GST pull down assay essentially as described (5). GST-p28, GST-MDM2 (*murine double minute 2*), and GST alone were bound to glutathione-Sepharose 4B beads (GE Healthcare) and unbound peptide was removed by washing with PBS. Whole-cell lysates of MCF-7 cells were mixed with beads, incubated for 2 h at 4°C, membranes washed twice with PBS, and boiled in SDS sample buffer before loading on 10% SDS-PAGE. Membranes were then incubated with skim milk (5%) in Tris-0.05% Tween 20 and polyclonal p53 antibody (FL-393; Santa Cruz Biotechnology), washed three times with Tris-0.05% Tween 20, secondary rabbit IgG-horseradish peroxidase antibody (Sigma-Aldrich) applied, and incubated for 1 h at room temperature. Potential binding sites on p53 were identified as follows. A GST pull-down assay in the presence of p28 (10-50 molar excess) was used to analyze interaction at the MDM2-binding site (19-26 amino acids) of p53; p53 bands were detected by immunoblotting with three anti-p53 antibodies, pAb1801 (32-79 amino acids; Santa Cruz Biotechnology), Ab2433 (277-296 amino acids; Abcam), and pAb1802 (306-393 amino acids; Santa Cruz Biotechnology), which represented the broadest coverage of the native p53 protein commercially available. After incubation, samples were washed twice with PBS to remove unbound p28, boiled in native PAGE sample buffer (Tri/glycerol/BPB), and loaded on 5% native PAGE. Samples were transferred to polyvinylidene difluoride membrane by electroblotting (0.2 Amp for 1 h) and membranes were incubated with a polyclonal antibody to p28 (1:5,000 dilution). After washing, horseradish peroxidase–conjugated rabbit anti-IgG antibody (1:7,000 dilution; Santa Cruz Biotechnology) was applied.

p28 regions binding to p53 were identified using competition between p28 and the p28 fragments p12, p18, and p18b for immobilized GST-p53. Reactions were incubated for 2 h at 4°C, washed twice with PBS to remove unbound p28, and loaded on 5% native PAGE. Polyvinylidene difluoride membranes were incubated with the polyclonal antibody to p28 at 4°C for 16 h. Band intensity was determined using Gel & Graph Digitizing Software, UN-SCAN-IT (Silk Scientific), and the ratio of specific protein to actin was calculated. Numbers displayed below each protein band are relative percentage (0 h expressed as 100%).

p53 DNA-Binding Activity

Nuclear fractions (Nuclear Extraction Kit; Active Motif) were isolated from MCF-7 cells after incubation with either 50 μmol/L p28 or azurin for 24 h according to the manufacturers' instructions. DNA-binding activity of p53 was analyzed using a TransAM p53 kit (Active Motif). Briefly, binding buffer containing DTT and poly(dI-dC) was introduced to each well to prevent nonspecific binding to the p53 consensus oligonucleotide. Nuclear extracts treated with H_2O_2 or buffer only were applied to each well as positive and negative controls, respectively. p53 antibody (1:1,000 dilution) was applied and incubated for 1 h. After washing, secondary antibody conjugated with horseradish peroxidase was added. p53 binding to DNA was determined by absorbance at 450 and 655 nm.

Reverse Transcription-PCR

MCF-7 cells were exposed to 50 μmol/L of p28 for 16, 24, 48, and 72 h. RNA was extracted using QIAshredder and the RNeasy kit (Qiagen), and 1 μg RNA was used for reverse transcription with 500 ng oligo$(dT)_{12\text{-}18}$ and SuperScript III reverse transcriptase (Invitrogen) at 50°C for 50 min. The annealing temperature was 57°C (25 cycles). The primers used were as follows: p53 5′-CAGCCAAGTCTGTGACTTGCACGTAC-3′ and 5′-CTATGTCGAAAAGTGTTTCTGTCATC-3′ and glyceraldehyde-3-phosphate dehydrogenase 5′-ACCTGACCTGCCGTCTAGAA-3′ and 5′-TCCACCACCCTGTTGCTGTA-3′ (19). PCR products were electrophoresed on a 2% agarose gel and visualized with ethidium bromide.

Results

Peptide Entry into Human Breast Cancer Cells

Confocal images indicated that p28 preferentially penetrated human breast cancer cells, MCF-7, T47D, and ZR-75-1, relative to normal MCF-10A cells (Fig. 1A, *1*). FACS analysis confirmed that p28 entry into the three human breast cancer cell lines was ~2- to 3-fold higher than in MCF-10A cells (ref. 20; Fig. 1A, *2*). p28 entry into MCF-7 determined by FACS showed penetration of MCF-7 cells (V_{max}, 1.89 MFI/s; K_m, 144.3 μmol/L) and MCF-10A cells (V_{max}, 0.79 MFI/s; K_m, 99.4 μmol/L) was saturable and ~2.4 times faster in MCF-7 cells (Fig. 1B). Exposure of MCF-7 cells to methyl-β-cyclodextrin and filipin, which disrupt caveolae through cholesterol depletion, significantly inhibited the penetration of p28 (Fig. 1C, *1*). The microtubule-disrupting agent, nocodazole, which inhibits caveosome formation and transport, confirmed p28 penetration involves caveolae-mediated endocytosis (Fig. 1C, *1*). In contrast, chlorpromazine, amiloride, and sodium azide, inhibitors of clathrin-mediated endocytosis, macropinocytosis (Na^+/H^+ pump), and energy-dependent transport, respectively, had no effect on the penetration of p28 (Fig. 1C, *1*). Monensin, an inhibitor of late endosome/lysosome processing, also reduced the intracellular accumulation of p28 (Fig. 1C, *1*). The penetration of p28 into MCF-10A cells was also inhibited by methyl-β-cyclodextrin, filipin, nocodazole, and monensin but not by amiloride, chlorpromazine, and sodium azide (Fig. 1C, *2*). MCF-7 cells were also more sensitive to the effects of methyl-β-cyclodextrin (~2.1-fold higher), filipin (~1.2-fold

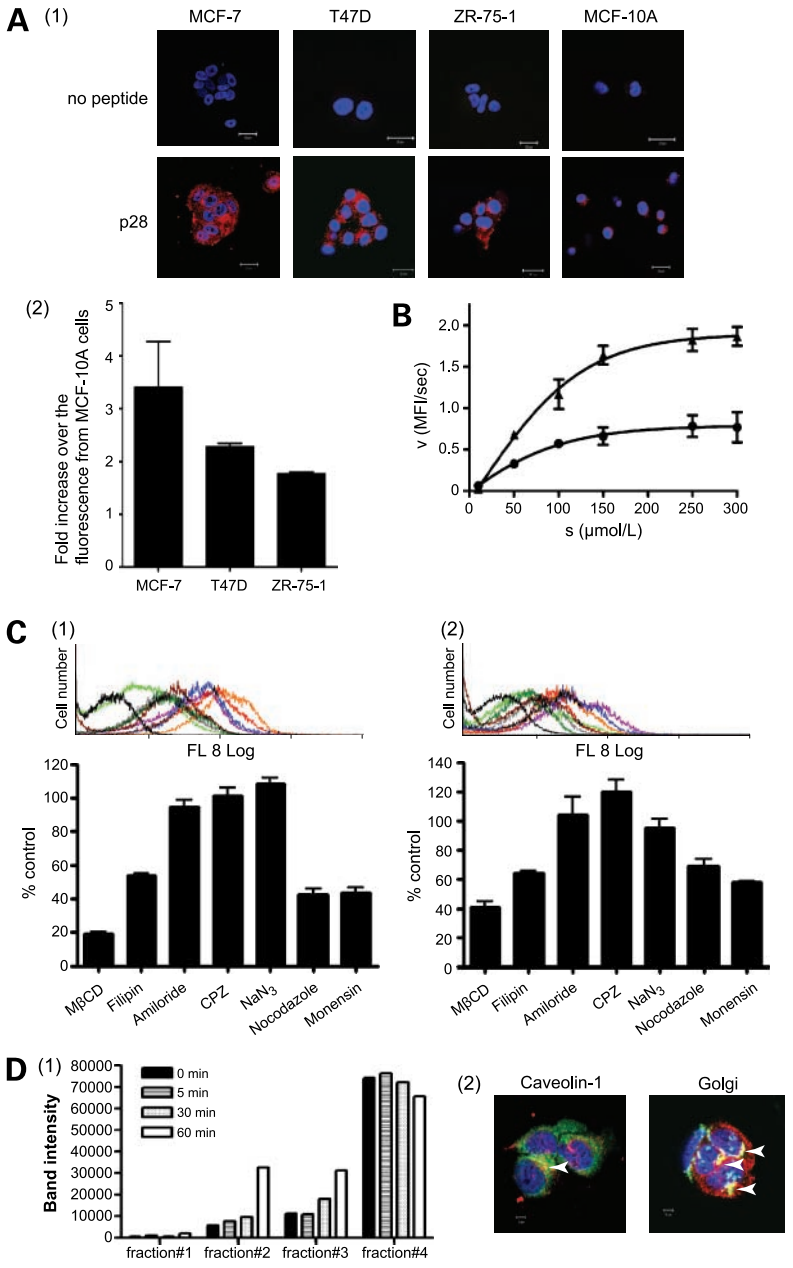

Figure 1. Preferential penetration of p28 into human breast cancer cells. **A,** human breast cell lines MCF-7, T47D, ZR-75-1, and MCF-10A were cultured with Alexa Fluor 568–labeled p28 at 37°C for 2 h and images were recorded by confocal microscopy (*1*). *Red,* Alexa Fluor 568–labeled p28; *blue,* 4′,6-diamidino-2-phenylindole (nucleus). Entry of p28 into human breast cancer MCF-7, T47D, and ZR-75-1 and normal MCF-10A cells at 37°C for 2 h was examined by FACS and MFI was determined with Summit V4.3 software. Values represent calculated fold increase over fluorescence from normal breast cells. Mean ± SE of three independent observations (*2*). **B,** kinetics of p28 entry into MCF-7 cells (*triangle*) relative to MCF-10A cells (*circle*) was determined by FACS (11). At least 10,000 cells were analyzed for each time point and concentration and MFI was calculated. K_m and V_{max} were determined by plotting p28 concentration (μmol/L) versus velocity (MFI/s). **C,** FACS analysis of p28 entry into MCF-7 and MCF-10A cells in the absence or presence of inhibitors. MCF-7 cells (*1*) and MCF-10A cells (*2*) were pretreated with inhibitors and incubated with 20 μmol/L Alexa Fluor 568–labeled p28. Negative control (no inhibitor/p28; *black*). Positive control (p28 only; *red*) was considered as 100%. Specific inhibitors included methyl-β-cyclodextrin (caveolae inhibitor 5 mmol/L, 60 min; *light green*), filipin (caveolae inhibitor 3 μg/mL, 60 min; *brown*), nocodazole (inhibits caveosome formation; 10 μmol/L, 60 min; *gray*), monensin (inhibits at late endosome/lysosome; 10 μmol/L, 60 min; *green*), chlorpromazine (inhibitor of clathrin-mediated endocytosis; 10 μg/mL, 60 min; *purple*), amiloride (macropinocytosis inhibitor; 50 μmol/L, 30 min; *blue*), and sodium azide (metabolic inhibitor; 1 mmol/L, 60 min; *orange*). Mean ± SE. **D,** immunoblotting of caveolin-1 (E249; Abcam) in MCF-7 cells. Fractions (*1,* 5%; *2,* 35% top layer; *3,* 35% bottom layer; *4,* 45% sucrose) were collected, separated on SDS-PAGE, and immunoblotted. Band intensity of caveolin-1 (22 kDa) was determined using Gel & Graph Digitizing Software, UN-SCAN-IT (*1*). Colocalization of p28 with caveolin-1 (*2*). MCF-7 cells cultured with Alexa Fluor 568–labeled p28 at 20 μmol/L were fixed and stained with anti–caveolin 1 antibody (Abcam; ref. 11). *Red,* Alexa Fluor 568–labeled p28; *blue,* 4′,6-diamidino-2-phenylindole (nucleus); *green,* caveolin-1; *yellow, arrowhead,* colocalization of p28 (*red*) with caveolin-1 (*green*). Confocal image for colocalization of Alexa Fluor 568–labeled p28 (*red*) with Golgi (*green*) in MCF-7 cells (*2*). Anti-golgin antibody was used for immunostaining (11). *Red,* Alexa Fluor 568–labeled p28; *blue,* 4′,6-diamidino-2-phenylindole (nucleus); *green,* Golgi; *yellow, arrowhead,* colocalization of p28 (*red*) with Golgi (*green*).

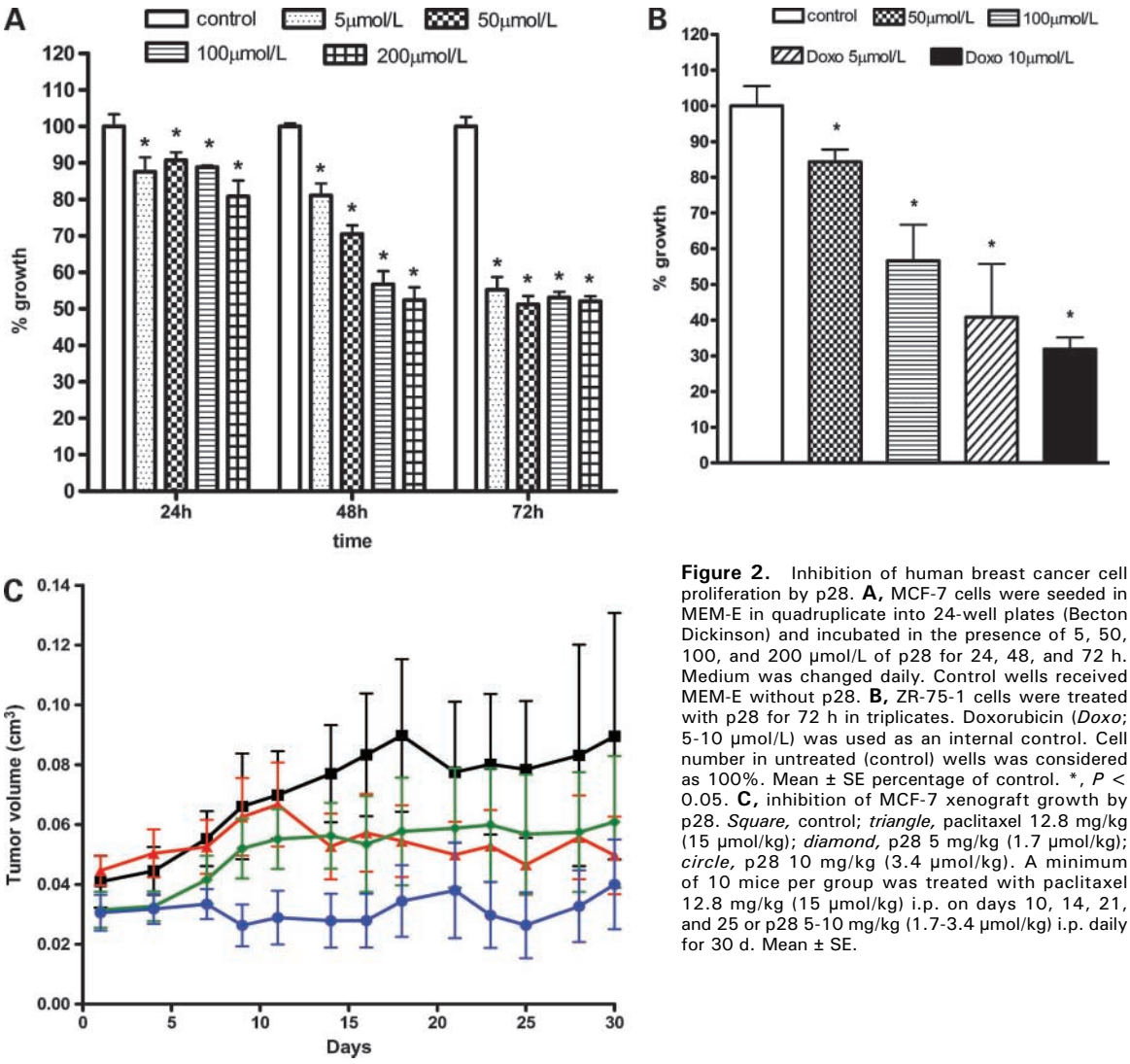

Figure 2. Inhibition of human breast cancer cell proliferation by p28. **A,** MCF-7 cells were seeded in MEM-E in quadruplicate into 24-well plates (Becton Dickinson) and incubated in the presence of 5, 50, 100, and 200 μmol/L of p28 for 24, 48, and 72 h. Medium was changed daily. Control wells received MEM-E without p28. **B,** ZR-75-1 cells were treated with p28 for 72 h in triplicates. Doxorubicin (*Doxo*; 5-10 μmol/L) was used as an internal control. Cell number in untreated (control) wells was considered as 100%. Mean ± SE percentage of control. *, $P < 0.05$. **C,** inhibition of MCF-7 xenograft growth by p28. *Square,* control; *triangle,* paclitaxel 12.8 mg/kg (15 μmol/kg); *diamond,* p28 5 mg/kg (1.7 μmol/kg); *circle,* p28 10 mg/kg (3.4 μmol/kg). A minimum of 10 mice per group was treated with paclitaxel 12.8 mg/kg (15 μmol/kg) i.p. on days 10, 14, 21, and 25 or p28 5-10 mg/kg (1.7-3.4 μmol/kg) i.p. daily for 30 d. Mean ± SE.

higher), and nocodazole (~1.6-fold higher) than MCF-10A (Fig. 1C), suggesting that although MCF-7 and MCF-10A may share similar routes of entry (caveolae-mediated and caveolae- and clathrin-independent mechanisms), the number of entry sites may be greater on (breast) cancer cells (11). Immunoblotting of caveolin-1 in MCF-7 cells revealed that the level of caveolin-1 was elevated in 35% sucrose fractions after exposure to p28 for 30 to 60 min (Fig. 1D), suggesting that p28 increased turnover of caveolae-mediated transport. Confocal images showed that p28 colocalized with caveolin-1 and golgin antibodies (Fig. 1D, 2), confirming their involvement in p28 entry and intracellular transport.

Effect of p28 Treatment on the Growth of Human Cancer Cells *In vitro* and *In vivo*

Azurin exerts its anticancer activity through induction of p53-mediated apoptosis (3, 5). Figure 2A and B illustrates the inhibitory effect of p28 on p53 wild-type MCF-7 and ZR-75-1 cells. The antiproliferative effect of p28 on MCF-7 cells was dose- and time-dependent ($P < 0.05$), decreasing cell number ~9.3%, ~29%, and ~50% at 50 μmol/L for 24, 48, and 72 h, respectively (Fig. 2A). p28 also inhibited ($P < 0.05$) the growth of ZR-75-1 cells, 16% at 50 μmol/L and 44% at 100 μmol/L after 72 h exposure, similar to the effect of 5 μmol/L doxorubicin (Fig. 2B). Moreover, p28 significantly reduced ($P < 0.05$) the volume of MCF-7 xenografts in athymic mice over the course of a daily 30-day i.p. exposure (Fig. 2C) without inducing either a loss in body weight or a behavioral change (data not shown). By day 30, 10 mg/kg (3.4 μmol/kg) p28 daily i.p. inhibited MCF-7 tumor growth ~20% more than 12.8 mg/kg (15 μmol/kg) paclitaxel over almost the entire course of the study. A reduction in BrdUrd labeling confirmed the reduction

Table 1. Effect of p28 on BrdUrd and p53 in MCF-7 xenograft tumors

	Tumors (*n*)	BrdUrd (%)	p53 (%)
Control	7	21.0 ± 2.7	15.6 ± 0.82
p28, 5 mg/kg (1.7 μmol/kg)	4	17.6 ± 0.75*	15.8 ± 0.51
p28, 10 mg/kg (3.4 μmol/kg)	3	16.1 ± 1.4*	17.7 ± 0.92
Paclitaxel, 12.8 mg/kg (15 μmol/kg)	6	9.0 ± 1.8*	25.4 ± 0.65*

NOTE: All tumors were collected on day 31 post-treatment. Mean ± SE.
*$P < 0.05$ (*t* test).

in cell proliferation (Table 1). The reduction in BrdUrd labeling and tumor volume was accompanied by a slight increase in nuclear p53 staining in p28 and a significant increase in the paclitaxel-treated groups compared with control (Table 1).

Inhibition of Cell Cycle Progression by p28

The rate of entry of p28 (11) into two isogenic human breast cancer cell lines, MCF-7 and MDD2 (Fig. 3A), was V_{max} 1.89 MFI/s (MCF-7) and 2.21 MFI/s (MDD2) and K_m 144.2 μmol/L (MCF-7) and 147.9 μmol/L (MDD2). Cell cycle analysis of the two cell lines revealed an increased cell population at the G_2-M phase after exposure to p28 for 48 to 72 h and subsequent induction of apoptosis (~22%) at 72 h in MCF-7 cells (Fig. 3B). In contrast, there was essentially no inhibition of cell cycle progression or apoptosis in MDD2 cells exposed to p28 (Fig. 3C), suggesting that any inhibition of proliferation by p28 was not likely to be a function or artifact of the amount of entry of p28 into the single breast epithelial cell line tested.

p53 Levels Are Elevated by p28

Azurin forms a complex with p53 and elevates intracellular p53 levels in MCF-7 cells (3, 5). Exposure of MCF-7 cells to p28 also markedly increased the intracellular level of p53 in MCF-7 cells with time of exposure (Fig. 4A). A GST pull-down assay suggested that p28 binds to p53 (Fig. 4B). Here, GST-p28 (10) and GST-MDM2 successfully pulled down p53 from MCF-7 cell lysates, but GST alone did not. We mapped the p53-interacting region of p28 using a similar assay and different fragments of p28. When GST-p53 protein immobilized on Sepharose 4B-glutathione beads was incubated with p28 and either p18 (amino acids 50-67), p18b (amino acids 60-77), or p12 (amino acids 66-77) of azurin, a significant amount of p28 was displaced by p18 and p18b, but only weakly when p12 was used as the competitor (Fig. 4C). These results suggest that maximal binding to p53 occurs within amino acids 11 to 18 of p28 (amino acids 60-67 of azurin), with the COOH-terminal 12 amino acids of p28 less efficient in binding p53.

The DNA-binding activity of p53 in nuclear extracts from MCF-7 cells treated with p28 or azurin was ~1.8- and ~2.3-fold higher than that from untreated control ($P > 0.1$, p28 versus azurin). The p53 wild-type consensus, but not the mutated oligonucleotide sequence, completely blocked the p28-induced increase in p53, confirming that the p53 in nuclear extracts of MCF-7 cells remains active, binding specifically to the consensus oligonucleotide sequence of p53 wild-type (Fig. 4D).

Stabilization of p53 by Prevention of Proteasomal Degradation

As the elevation in p53 in response to p28 exposure could result from either transcriptional activation of p53 or protein stabilization, we determined the level and time course of p53 expression in MCF-7 cells during exposure to p28. Reverse transcription-PCR showed that p53 transcription was not significantly altered after exposure to p28, suggesting that the increase in p53 occurred post-translationally (Fig. 5A). Computer modeling indicates that azurin binds, in part, to the NH_2-terminal region of p53 near MDM2, an E3 ubiquitin ligase (21) and major regulator of p53 degradation (22), suggesting that p28 could interfere with MDM2 binding to p53 (23). However, molar increases of p28 did not compete with GST-MDM2 for binding to p53 (Fig. 5B), suggesting that any p28-induced decrease in the ubiquitination of p53 was not via a MDM2-mediated pathway (Fig. 5C) and that amino acids 19 to 26 of p53, the MDM2-binding site (24), was not a preferred binding site for p28. The ladder of p53-specific high molecular weight and smear bands that result from ubiquitination of p53 (p53-Ub_n; refs. 17, 25), the main p53 degradation pathway, in the presence of the proteasome inhibitor MG132, was markedly reduced compared with untreated control when MCF-7 cells were exposed to p28 at 50 μmol/L for 24 h (Fig. 5C). The inhibitory effect was increased and extended 48 h post-exposure to p28 when the proteasome inhibitor MG132 was incorporated into the reaction. At 72 h, the level of p53-Ub_n was slightly higher than control. Because p28 continued to accumulate p53 after 72 h exposure (~332%; Fig. 4A), the slightly higher level of p53 may provide substrate for several additional known E3 ubiquitin ligases promoting degradation by the proteasome pathway. In sum, the results suggest that the p28-induced increase in p53 levels resulted from stabilizing p53 through decreased ubiquitination and proteasomal degradation rather than transcriptional activation.

An additional GST pull-down assay in the presence or absence of p53 antibodies, which recognize different motifs of the p53 protein (amino acids 32-79, 277-296, and 306-393), did not block p28 binding to p53. This suggests that p28 binds to a region of p53 outside these recognition sites

(Fig. 5D) but within a region bounded by either amino acids 1 to 18, 27 to 31, 80 to 276, or 297 to 305.

Modulation of Cell Cycle–Related Proteins by p28

Upregulation of the CDK inhibitors p21 and p27 blocks cell cycle progression (26). p28 increased intracellular levels of p21, p27, CDK6, and cyclin B1 over control in MCF-7 cells with time post-exposure (Fig. 6A). The levels of CDK2 and cyclin A, essential proteins in the mitotic process (27), decreased with time post-exposure of MCF-7 cells to p28 (Fig. 6A). In contrast, p53, cdc2, CDK2, CDK4, and CDK6 essentially remained constant in MDD2 cells (Fig. 6A), whereas cyclin A and cyclin B1 (48 h) increased slightly. Because p21 can be expressed by a p53-independent pathway in MDD2 cells (28, 29), p21 remained detectable. However, p28 did not alter the level of p21 (Fig. 6A). In contrast, p27 was not detectable in

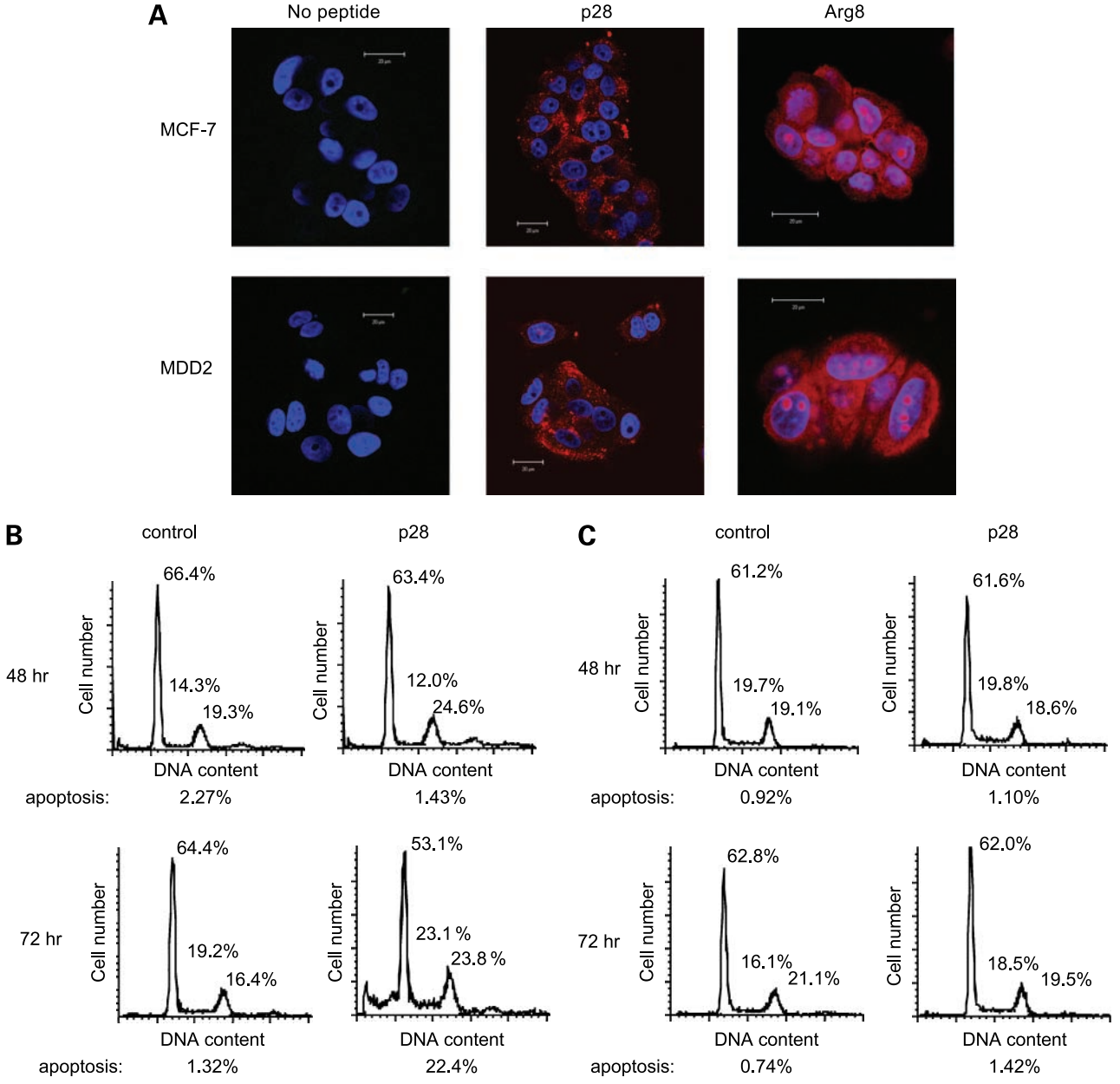

Figure 3. p28 penetration and effect on cell cycle of isogenic breast cancer cell lines. **A,** MCF-7 and MDD2 cells cultured on coverslips overnight in phenol red–free MEM were treated with 20 μmol/L p28 or 10 μmol/L octa-arginine (Arg_8) for 2 h at 37°C. Images were taken by confocal microscopy (LSM 510) ×63 at λ_{ex} 364, 488, and 568 nm. *Red,* Alexa Fluor 568–labeled p28; *blue,* 4′,6-diamidino-2-phenylindole (nucleus). MCF-7 cells (**B**) and MDD2 cells (**C**) were treated with p28 (50 μmol/L) for 48 and 72 h. Fixed cells were stained with propidium iodide and DNA content was analyzed by flow cytometry. The percentage of cells in the G_1, S, G_2-M, and sub-G_1 (apoptosis) phases are indicated.

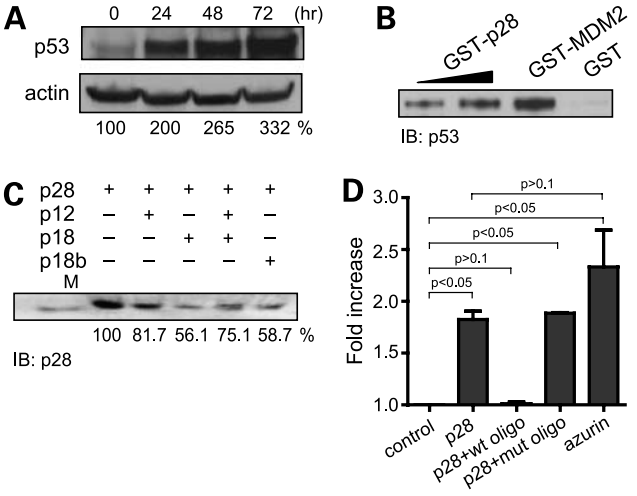

Figure 4. Interaction of p28 with p53. **A,** p53 levels in MCF-7 cells with time after incubation with p28. Percent change relative to p53 level immediately before treatment (0 h as 100%). **B,** GST pull-down assay showing complex formation between GST-p28 and p53. *Left* to *right,* GST-p28 (10 and 20 μg/reaction), GST-MDM2 (20 μg/reaction), and GST alone (20 μg/reaction). p53 was detected by immunoblotting using anti-p53 antibody. **C,** competition for p28 binding to GST-p53 by a molar excess of p28 fragments p12, p18, and p18b. Relative amount of binding (p28 alone expressed as 100%). *M,* p28 marker. **D,** p53 DNA-binding activity assay in MCF-7 nuclear extracts after exposure to p28 or azurin. Nuclear extracts of H_2O_2-treated MCF-7 cells served as an internal control. The p53-oligonucleotide complex was quantified with a monoclonal antibody to p53. Mean ± SE of triplicates.

untreated or p28-exposed MDD2 cells. The increased levels of p21 and cyclin B1 in MCF-7 cells detected by immunoblotting in response to p28 are reflected by their increase in nuclear and cytosolic compartments, respectively (Fig. 6B and C). Exposure of MCF-7 cells to p28 also induced the accumulation of phosphorylated cdc2, the inactive form of cdc2 (30), which did not increase following exposure of MDD2 cells to p28 (Fig. 6D).

Discussion

Amino acids 50 to 77 of azurin (p28) exhibit preferential penetration and an antiproliferative effect on human breast cancer cells mediated by p53, a tumor suppressor protein that becomes functionally active in response to stress and triggers either cell cycle arrest or apoptotic cell death (31). We and others using a series of GST pull-down assays (5), glycerol gradient centrifugation (2, 3), microcalorimetry (7), single-molecule force spectroscopy (8), and computer modeling (9, 23) have reported that azurin binds within either the NH_2-terminal domain or the DBD of p53 and increases its intracellular levels (3, 5, 7). Our suggestion that the azurin-binding domain for p53 includes a hydrophobic patch described by azurin Met^{44} and Met^{64} is supported by the observation that a disrupted hydrophobic patch mutant (mutant azurin M44KM64E) is less cytotoxic to human melanoma (Mel-2) cells than wild-type azurin (3). This suggests that the p53-binding domain of the azurin molecule surrounds the hydrophobic patch. A recent docking simulation study showed a significant loss of ~75 kJ/mol in the interaction free energy of the mutant complex with respect to wild-type azurin (9), again indicating that the hydrophobic patch of azurin surrounding residues Met^{44} and Met^{64} is important for interaction with p53. As Met^{64} resides within the p53-binding site of p28 (amino acid 15 of p28), our competition assays, mutant studies, and docking experiments clearly suggest that this is the azurin domain that binds to p53. Interestingly, this is also the region we identified as the protein transport domain for azurin entry into cells (11).

The increase in p53 in response to p28 occurs post-translationally and essentially results from a reduction in proteasome degradation of p53. As p53 stability is predominantly regulated through the ubiquitin-proteasomal pathway, identification of molecules that block ubiquitination of p53 is a promising therapeutic strategy for the treatment of cancers. Small molecules such as the *cis*-imidazole analogue Nutlin and HLI98, which interfere with p53:MDM2 interaction and inhibit the E3 ubiquitin ligase activity of MDM2, respectively, have been screened for potential as cancer therapeutics (32, 33). Recent studies have shown that, among the known ubiquitin ligases for p53, MDM2, COP1, Pirh2, ARF-BP1, and possibly Parc and TOPORS are expressed in breast cancer cells where they directly interact with p53 and promote ubiquitination and degradation (34–38). Interestingly, COP1 is significantly overexpressed in breast and ovarian cancers (39) and ARF-BP1 is also highly expressed in 80% of breast cancer cell lines including MCF-7 and T47D, whereas its expression level in normal breast MCF-10A is negligible (38). Although the binding region(s) of TOPORS and ARF-BP1 on p53 remains undetermined, it has been suggested that COP1 associates within the central to COOH-terminal domain of p53 (40). Pirh2 has been reported to interact within the region bounded by amino acids 82 to 292 in the p53 DBD (40). Parc (a Parkin-like ubiquitin ligase) appears to bind within the COOH-terminal region of p53 (amino acids 290-393; refs. 36, 41). Because p28 does not bind to the NH_2-terminal MDM2-binding region (Fig. 5B) or the COOH-terminal region of p53 (Fig. 5D), it suggests that p28 does not inhibit the binding of either MDM2 or possibly Parc to p53. Taken together, the data suggest that p28 binds within amino acids 80 to 276 of the p53 DBD and interferes with the interaction between p53 and the ubiquitin ligases Pirh2, COP1, and possibly TOPORS and ARF-BP1, thereby leading to a decrease in the ubiquitination and degradation of p53. This suggestion fits well with computer modeling data suggesting that azurin binds to the flexible L_1 (amino acids 113-115) and s_7-s_8 (amino acids 221 and 224-229) loops of the p53 DBD and stabilizes them through protein-protein tight packing (9). As the L_1 and s_7-s_8 loops are the most unstable regions in the p53 DBD due to their very loose packing against each other or against the β-sheet core, it results in very high mobility. This conformational flexibility plays a key role in determining macromolecular recognition specificity, allowing

for high efficiency and rapid turnover of protein-protein interactions (9). Although the L_1 and s_7-s_8 regions also associate with the β_1-β_2 and β_7-β_8 sheets in azurin, which do not incorporate the p28 region (9), amino acids Met^{64}, Leu^{68}, and Tyr^{72} are included within the p53 DBD azurin-binding region and are within amino acids 60-77 (p18b) of azurin.

The tumor suppressor protein, p53, is a predominantly nuclear protein that acts as a transcriptional regulator for the 21-kDa protein $p21^{Waf1/Cip1}$, an inhibitor of cell cycle progression (31, 42). Treatment of MCF-7 cells with p28 increased p53 levels, leading to higher intracellular levels of p21, a strong inhibitor of CDK activity, especially cdc2 and CDK2 that regulate cell cycle progression at G_1 and G_2-M, respectively. In the progression through G_2-M, cdc2 and CDK2 kinases are activated primarily in association with cyclin B and cyclin A (27). The CDK inhibitor p21 associates with cyclin A in G_2-M–arrested cells (42). Under the same conditions, cyclin B1 does not associate with p21 and the level of cyclin B1 increases continuously (42). This suggests that the p28-induced G_2-M arrest in MCF-7 cells is associated with inhibition of CDK2 and cyclin A (Fig. 6A). The p28-induced increase in p21 in MCF-7 cells was also accompanied by a time-dependent increase in p27, another member of the Cip/Kip CDK inhibitor family. Hsu et al. (43) recently showed that induction of p53 increased both p21 and p27 promoter activity. In addition, p53 DNA-binding activity of the p21 and p27 promoters is reportedly activated by the p53 inducer, progesterone, suggesting that not only p21 but also p27 is transcriptionally regulated by p53 (43). Collectively, our data suggest that enhancement of p53 levels subsequently upregulates p21 and p27, inducing a significant decrease in intracellular CDK2 and cyclin A levels in MCF-7 cells and inhibition of the cell cycle at G_2-M (Fig. 6A). The reported lack of or inefficient association between cyclin B1 and p21 (42) suggests that the increase in cyclin B1 following exposure to p28 may reflect a similar pattern following a p28-induced increase in p21. An increase in phosphorylated cdc2 (inactive form) following exposure

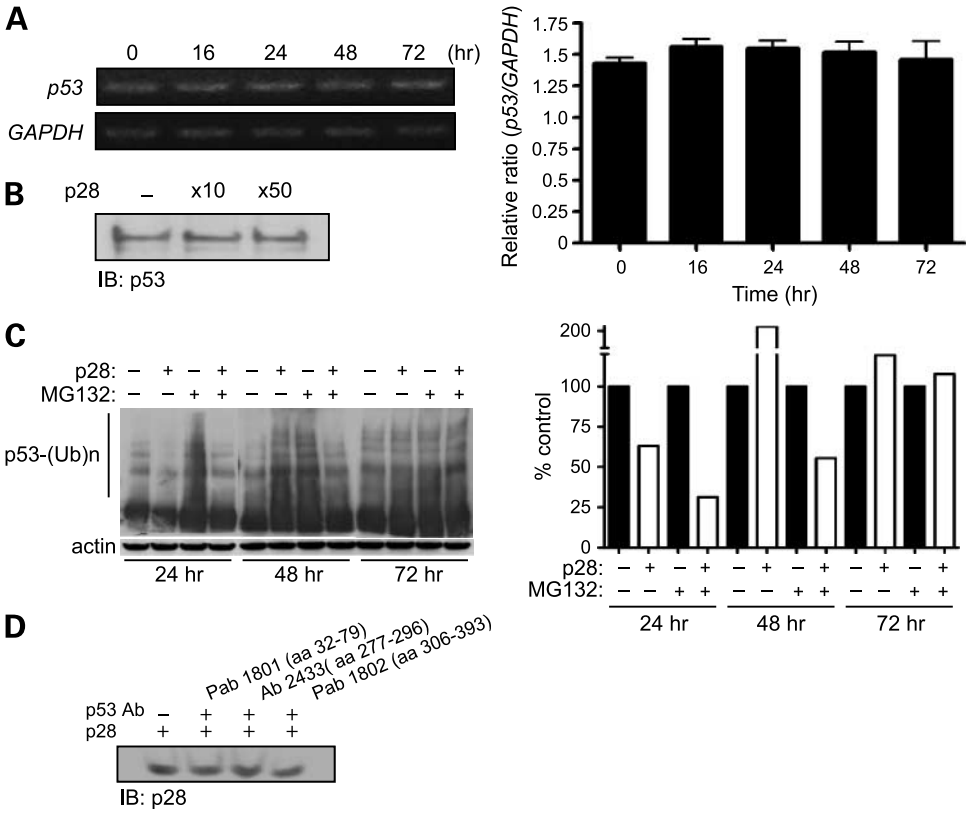

Figure 5. Stabilization of p53 by p28. **A,** RNA extracted from MCF-7 cells exposed to p28 for 16, 24, 48, and 72 h. mRNA levels of *p53* and glyceraldehyde-3-phosphate dehydrogenase (*GAPDH*) as an internal control gene were determined by reverse transcription-PCR analysis. p53 bands were quantified and normalized against glyceraldehyde-3-phosphate dehydrogenase. Mean ± SE of triplicate assays. **B,** p53 was pulled down by GST-MDM2 in the presence of a molar excess of p28. Protein samples were loaded on SDS-PAGE and p53 was detected by immunoblotting using anti-p53 antibody. **C,** MCF-7 cells were exposed to p28 at 50 μmol/L for 24, 48, and 72 h in absence or presence of proteasome inhibitor MG132. The position of the p53-ubiquitin conjugates (p53-Ub_n) is indicated. The histogram shows relative amounts of p53-Ub_n (untreated control samples at each time point expressed as 100%). **D,** three different anti-p53 antibodies, pAb1801 (32-79 amino acids), Ab2433 (277-296 amino acids), and pAb1802 (306-393 amino acids), reacted with GST-p53 immobilized beads in the presence of p28. p28 was detected by immunoblotting using an anti-p28 antibody.

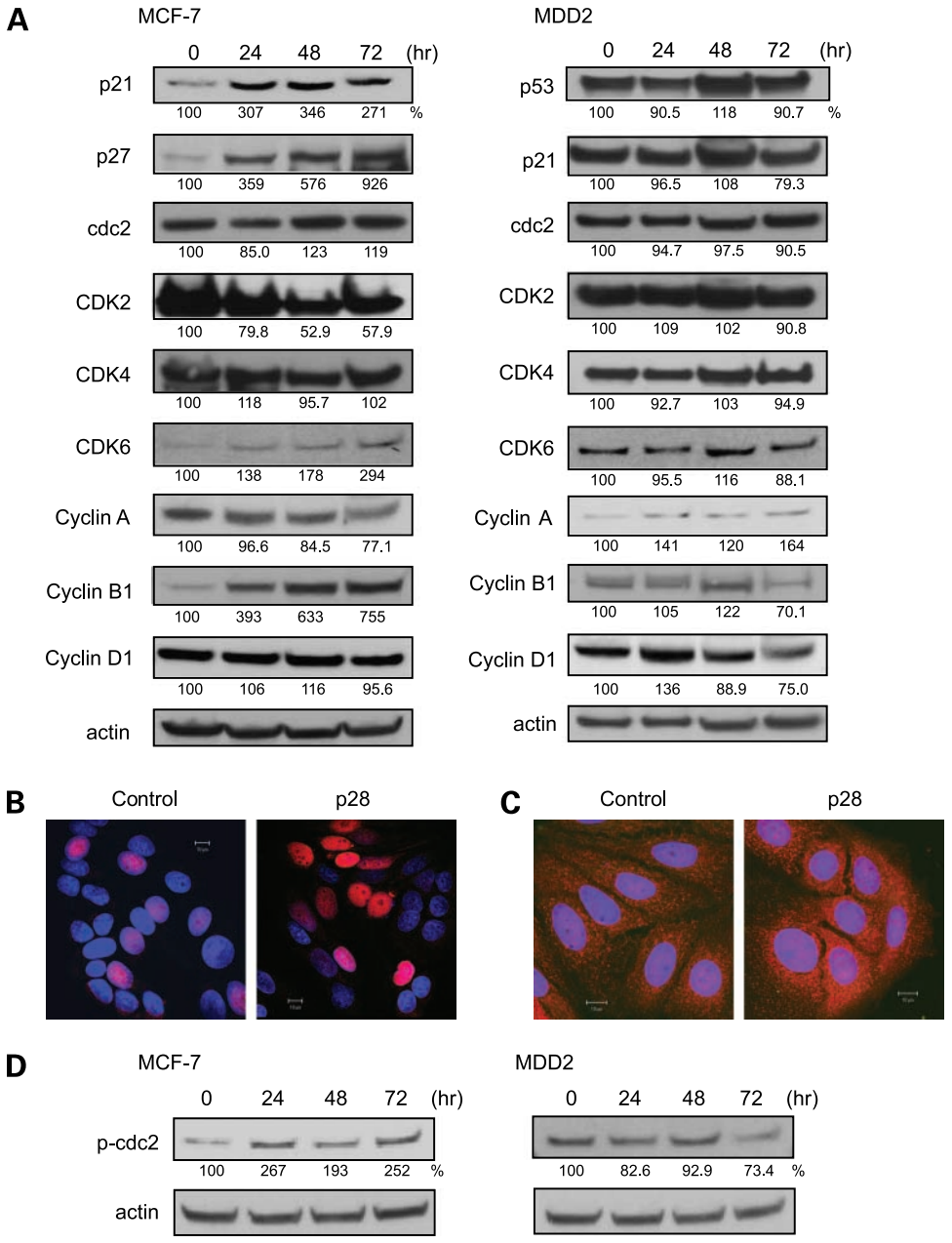

Figure 6. Induction of the cyclin (CDK and CDK inhibitor) cascade by p28. **A,** MCF-7 cells (*left*) and MDD2 cells (*right*) were exposed to p28 (50 μmol/L) for 24, 48, and 72 h and protein levels were determined by immunoblotting. Intracellular localization and relative level of p21 (**B**) and cyclin B1 (**C**) in MCF-7 cells exposed to p28 (50 μmol/L) for 72 h. **D,** level of phosphorylated cdc2 was determined with an anti-phosphorylated cdc2 antibody in MCF-7 cells (*left*) and MDD2 cells (*right*). All results normalized by actin as an internal control (**A** and **D**).

to p28 accompanied the increased cellular level of cyclin B1, suggesting that the increase in the cdc2-cyclin B complex reflects the increase in cdc2 phosphorylation (30, 44, 45). Nocodazole, a known disruptor of microtubules and transcriptional and translational activator of p21, also induces a similar G_2 arrest in MCF-7 and MDA-MB-468 human breast cancer cells, accompanied by high levels of cytoplasmic cyclin B1 (46). Differentiation agents such as all-*trans* retinoic acid and sodium butyrate produce growth inhibition and the G_1 arrest in oral squamous carcinoma cells, which correlates with the induction of G_1-phase cell cycle regulatory proteins CDK6, p21, and p27 and the inhibition of the G_2-phase cell cycle regulatory protein CDK2 (47). Because p28 did not enhance p21 in MDD2 cells, and p27 appears absent in these cells, the levels of CDK2 and cyclin A were not significantly altered (Fig. 6A) and no inhibition of cell cycle occurred. Additional evidence for a p28-induced decrease in the CDK2 and cyclin A complex, a key regulator of cdc2 activity in human cells that causes a G_1 and G_2-M arrest (48, 49), is found in the G_2 delay that follows cyclin A RNA interference introduction to HeLa cells (50). This inactivates the CDK2-cyclin A complex, causing cell cycle arrest in G_2-M.

Our observations suggest that p28 binds to p53, possibly within a hydrophobic DBD (amino acids 80-276), stabilizing the protein and increasing p53 levels by decreasing proteasomal degradation. It subsequently upregulates p21 and p27 and inactivates the CDK2-cyclin A complex, thereby causing a G_2-M cell cycle arrest in MCF-7 breast cancer cells. Its preferential penetration of human solid tumor cells (11) and prevention of p53 degradation through MDM2- and Parc-independent pathways suggest that p28 and similar peptides may provide a novel source of cytostatic and cytotoxic (apoptotic) agents in the treatment of breast cancer.

Disclosure of Potential Conflicts of Interest

CDG Therapeutics has an exclusive licensing agreement for the development and commercialization of cupredoxin-derived peptides. T. Yamada is one of the inventors and potentially will receive a share of the royalty received by University of Illinois at Chicago through the licensing of the technology. C.W. Beattie is Chief Scientific Officer of CDG Therapeutics. All terms of the sponsored research agreements are managed by University of Illinois at Chicago in accordance with its conflict of interest management policies. T.K. Das Gupta is a cofounder of CDG Therapeutics and shareholder in it.

Acknowledgments

We thank Dr. Yan-Hwa Wu Lee (Institute of Biochemistry, National Yang-Ming University) for p53 plasmid DNA.

References

1. De Rienzo F, Gabdoulline RR, Menziani MC, Wade RC. Blue copper proteins: a comparative analysis of their molecular interaction properties. Protein Sci 2000;9:1439–54.

2. Yamada T, Goto M, Punj V, et al. The bacterial redox protein azurin induces apoptosis in J774 macrophages through complex formation and stabilization of the tumor suppressor protein p53. Infect Immun 2002;70:7054–62.

3. Yamada T, Goto M, Punj V, et al. Bacterial redox protein azurin, tumor suppressor protein p53, and regression of cancer. Proc Natl Acad Sci U S A 2002;99:14098–103.

4. Yamada T, Hiraoka Y, Ikehata M, et al. Apoptosis or growth arrest: modulation of tumor suppressor p53's specificity by bacterial redox protein azurin. Proc Natl Acad Sci U S A 2004;101:4770–5.

5. Punj V, Bhattacharyya S, Saint-Dic D, et al. Bacterial cupredoxin azurin as an inducer of apoptosis and regression in human breast cancer. Oncogene 2004;23:2367–78.

6. Yang DS, Miao XD, Ye ZM, et al. Bacterial redox protein azurin induce apoptosis in human osteosarcoma U2OS cells. Pharmacol Res 2005;52:413–21.

7. Apiyo D, Wittung-Stafshede P. Unique complex between bacterial azurin and tumor-suppressor protein p53. Biochem Biophys Res Commun 2005;332:965–8.

8. Taranta M, Bizzarri AR, Cannistraro S. Probing the interaction between p53 and the bacterial protein azurin by single molecule force spectroscopy. J Mol Recognit 2008;21:63–70.

9. De Grandis V, Bizzarri AR, Cannistraro S. Docking study and free energy simulation of the complex between p53 DNA-binding domain and azurin. J Mol Recognit 2007;20:215–26.

10. Yamada T, Fialho AM, Punj V, Bratescu L, Das Gupta TK, Chakrabarty AM. Internalization of bacterial redox protein azurin in mammalian cells: entry domain and specificity. Cell Microbiol 2005;7:1418–31.

11. Taylor BN, Mehta RR, Yamada T, et al. Noncationic peptides obtained from azurin preferentially enter cancer cells. Cancer Res 2009;69:537–46.

12. Mi Q, Lantvit D, Reyes-Lim E, et al. Evaluation of the potential cancer chemotherapeutic efficacy of natural product isolates employing *in vivo* hollow fiber tests. J Nat Prod 2002;65:842–50.

13. Shilkaitis A, Green A, Punj V, Steele V, Lubet R, Christov K. Dehydroepiandrosterone inhibits the progression phase of mammary carcinogenesis by inducing cellular senescence via a p16-dependent but p53-independent mechanism. Breast Cancer Res 2005;7:R1132–40.

14. Razandi M, Oh P, Pedram A, Schnitzer J, Levin ER. ERs associate with and regulate the production of caveolin: implications for signaling and cellular actions. Mol Endocrinol 2002;16:100–15.

15. Zivadinovic D, Watson CS. Membrane estrogen receptor-α levels predict estrogen-induced ERK1/2 activation in MCF-7 cells. Breast Cancer Res 2005;7:R130–44.

16. Tsukamoto S, Yamashita K, Tane K, et al. Girolline, an antitumor compound isolated from a sponge, induces G_2-M cell cycle arrest and accumulation of polyubiquitinated p53. Biol Pharm Bull 2004;27:699–701.

17. Kitagaki J, Agama KK, Pommier Y, Yang Y, Weissman AM. Targeting tumor cells expressing p53 with a water-soluble inhibitor of Hdm2. Mol Cancer Ther 2008;7:2445–54.

18. Di Stefano V, Blandino G, Sacchi A, Soddu S, D'Orazi G. HIPK2 neutralizes MDM2 inhibition rescuing p53 transcriptional activity and apoptotic function. Oncogene 2004;23:5185–92.

19. Zhao Y, Katzman RB, Delmolino LM, et al. The notch regulator MAML1 interacts with p53 and functions as a coactivator. J Biol Chem 2007;282:11969–81.

20. Tait L, Soule HD, Russo J. Ultrastructural and immunocytochemical characterization of an immortalized human breast epithelial cell line, MCF-10. Cancer Res 1990;50:6087–94.

21. Haupt Y, Maya R, Kazaz A, Oren M. MDM2 promotes the rapid degradation of p53. Nature 1997;387:296–9.

22. Haupt S, Louria-Hayon I, Haupt Y. p53 licensed to kill? Operating the assassin. J Cell Biochem 2003;88:76–82.

23. Taranta M, Bizzarri AR, Cannistraro S. Modeling the interaction between the N-terminal domain of the tumor suppressor p53 and azurin. J Mol Recognit 2009;22:215–22.

24. Courtois S, de Fromentel CC, Hainaut P. p53 protein variants: structural and functional similarities with p63 and p73 isoforms. Oncogene 2004;23:631–8.

25. Dai MS, Lu H. Inhibition of MDM2-mediated p53 ubiquitination and degradation by ribosomal protein L5. J Biol Chem 2004;279:44475–82.

26. Vidal A, Koff A. Cell-cycle inhibitors: three families united by a common cause. Gene 2000;247:1–15.

27. Lu YJ, Yang SH, Chien CM, et al. Induction of G_2-M phase arrest and apoptosis by a novel enediyne derivative, THDB, in chronic myeloid leukemia (HL-60) cells. Toxicol In Vitro 2007;21:90–8.

28. Haidara K, Zamir L, Shi QW, Batist G. The flavonoid Casticin has multiple mechanisms of tumor cytotoxicity action. Cancer Lett 2006;242:180–90.

29. Gartel AL, Najmabadi F, Goufman E, Tyner AL. A role for E2F1 in Ras activation of p21(WAF1/CIP1) transcription. Oncogene 2000;19:961–4.

30. Gaul L, Mandl-Weber S, Baumann P, Emmerich B, Schmidmaier R. Bendamustine induces G_2 cell cycle arrest and apoptosis in myeloma cells: the role of ATM-Chk2-25A and ATM-p53-21-pathways. J Cancer Res Clin Oncol 2008;134:245–53.

31. Vogelstein B, Lane D, Levine AJ. Surfing the p53 network. Nature 2000;408:307–10.

32. Chen D, Brooks CL, Gu W. ARF-BP1 as a potential therapeutic target. Br J Cancer 2006;94:1555–8.

33. Shangary S, Wang S. Small-molecule inhibitors of the MDM2-53 protein-protein interaction to reactivate p53 function: a novel approach for cancer therapy. Annu Rev Pharmacol Toxicol 2009;49:223–41.

34. Kubbutat MH, Jones SN, Vousden KH. Regulation of p53 stability by Mdm2. Nature 1997;387:299–303.

35. Brooks C, Gu W. Dynamics in the p53-2 ubiquitination pathway. Cell Cycle 2004;3:895–9.

36. Nikolaev AY, Gu W. PARC: a potential target for cancer therapy. Cell Cycle 2003;2:169–71.

37. Rajendra R, Malegaonkar D, Pungaliya P, et al. Topors functions as an E3 ubiquitin ligase with specific E2 enzymes and ubiquitinates p53. J Biol Chem 2004;279:36440–4.

38. Chen D, Kon N, Li M, Zhang W, Qin J, Gu W. ARF-BP1/Mule is a critical mediator of the ARF tumor suppressor. Cell 2005;121:1071–83.

39. Dornan D, Bheddah S, Newton K, et al. COP1, the negative regulator

of p53, is overexpressed in breast and ovarian adenocarcinomas. Cancer Res 2004;64:7226–30.

40. Corcoran C, Huang Y, Sheikh M. The p53 paddy wagon: COP1, Pirh2 and MDM2 are found resisting apoptosis and growth arrest. Cancer Biol Ther 2004;3:721–5.

41. Nikolaev A, Li M, Puskas N, Qin J, Gu W. Parc: a cytoplasmic anchor for p53. Cell 2003;112:29–40.

42. Bates S, Ryan K, Phillips A, Vousden K. Cell cycle arrest and DNA endoreduplication following $p21^{Waf1/Cip1}$ expression. Oncogene 1998; 17:1691–703.

43. Hsu SP, Ho PY, Juan SH, Liang YC, Lee WS. Progesterone inhibits human endothelial cell proliferation through a p53-dependent pathway. Cell Mol Life Sci 2008;65:3839–50.

44. Parker LL, Piwnica-Worms H. Inactivation of the p34cdc2-cyclin B complex by the human WEE1 tyrosine kinase. Science 1992;257:1955–7.

45. Mueller PR, Coleman TR, Kumagai A, Dunphy WG. Myt1: a membrane-associated inhibitory kinase that phosphorylates Cdc2 on both threonine-14 and tyrosine-15. Science 1995;270:86–90.

46. Blajeski AL, Phan VA, Kottke TJ, Kaufmann SH. G(1) and G(2) cell-cycle arrest following microtubule depolymerization in human breast cancer cells. J Clin Invest 2002;110:91–9.

47. Wang A, Zeng R, Huang H. Retinoic acid and sodium butyrate as cell cycle regulators in the treatment of oral squamous carcinoma cells. Oncol Res 2008;17:175–82.

48. Gray N, Detivaud L, Doerig C, Meijer L. ATP-site directed inhibitors of cyclin-dependent kinases. Curr Med Chem 1999;6:859–75.

49. Furuno N, den Elzen N, Pines J. Human cyclin A is required for mitosis until mid prophase. J Cell Biol 1999;147:295–306.

50. Mitra J, Enders GH. Cyclin A/Cdk2 complexes regulate activation of Cdk1 and Cdc25 phosphatases in human cells. Oncogene 2004;23: 3361–7.